

Multiple Exciton Generation in Chiral Carbon Nanotubes: Density Functional Theory Based Computation

Andrei Kryjevski, Deyan Mihaylov

Department of Physics, North Dakota State University, Fargo, ND 58108, USA

Svetlana Kilina, Dmitri Kilin

Department of Chemistry, North Dakota State University, Fargo, ND 58108, USA

(Dated: December 19, 2021)

Abstract

We use Boltzmann transport equation (BE) to study time evolution of a photo-excited state in a nanoparticle including phonon-mediated exciton relaxation and the multiple exciton generation (MEG) processes, such as exciton-to-biexciton multiplication and biexciton-to-exciton recombination. BE collision integrals are computed using Kadanoff-Baym-Keldysh many-body perturbation theory (MBPT) based on density functional theory (DFT) simulations, including exciton effects. We compute internal quantum efficiency (QE), which is the number of excitons generated from an absorbed photon in the course of the relaxation. We apply this approach to chiral single-wall carbon nanotubes (SWCNTs), such as (6,2), and (6,5). We predict efficient MEG in the (6,2) and (6,5) SWCNTs within the solar spectrum range starting at the $2E_g$ energy threshold and with QE reaching ~ 1.6 at about $3E_g$, where E_g is the electronic gap.

I. INTRODUCTION

Efficiency of photon-to-electron energy conversion in nanomaterials is an important issue that has been actively investigated in recent years. For instance, it is envisioned that efficiency of the nanomaterial-based solar cells can be increased due to carrier multiplication, or multiple exciton generation (MEG) process, where absorption of a single energetic photon results in the generation of several excitons [1–3]. In the course of MEG the excess photon energy is diverted into creating additional charge carriers instead of generating atomic vibrations [3]. In fact, phonon-mediated electron relaxation is a major time-evolution channel competing with the MEG. The conclusion about MEG efficiency in a nanoparticle can only be made by simultaneously including MEG, phonon-mediated carrier relaxation, and, potentially, other processes, such as charge and energy transfer [4, 5].

In the bulk semiconductor materials MEG in the solar photon energy range is known to be inefficient [6–8]. In contrast, in nanomaterials MEG is expected to be enhanced by spatial confinement, which increases electrostatic electron interactions [3, 9–12]. Internal quantum efficiency (QE) is the average number of excitons generated from an absorbed photon. It is a potent measure of MEG efficiency. QE exceeding 100% has been measured in recent experiments on, *e.g.*, silicon and germanium nanocrystals, and in nanoparticle-based solar cells [13–18].

Also, MEG has been observed in single-wall carbon nanotubes (SWCNTs) using transient absorption spectroscopy [14] and the photocurrent spectroscopy [19]; $QE = 1.3$ at the photon energy $\hbar\omega = 3E_g^{opt}$, where E_g^{opt} is the optical gap, was found in the (6,5) SWCNT. Theoretically, MEG in SWCNTs has been investigated using tight-binding approximation with QE up to 1.5 predicted in (17,0) zigzag SWCNT [20, 21]. It is understood that in semiconductor nanostructures MEG is dominated by the impact ionization process [22, 23]. Therefore, MEG QE requires calculations of the exciton-to-biexciton decay rate ($R_{1\rightarrow 2}$) and of the biexciton-to-exciton recombination rate ($R_{2\rightarrow 1}$), the direct Auger process, and, of course, inclusion of carrier phonon-mediated relaxation. In quasi one-dimensional systems, such as SWCNTs, accurate description of these processes requires inclusion of the electron-hole bound state effects – excitons [24].

Recently, Density Functional Theory (DFT) combined with the many-body perturbation theory (MBPT) techniques has been used to calculate $R_{1\rightarrow 2}$ and $R_{2\rightarrow 1}$ rates, and the photon-

to-bi-exciton, R_2 , and photon-to-exciton, R_1 , rates in two chiral (6,2) and (10,5) SWCNT which have different diameters, including exciton effects [25]. QE was then estimated as $QE = (R_1 + 2R_2)/(R_1 + R_2)$. However, phonon relaxation was not included. Also, $R_{1 \rightarrow 2}$ and $R_{2 \rightarrow 1}$ for the singlet fission (SF) channel of MEG for these systems have been computed in [26]. The results suggested that efficient MEG in chiral SWCNTs, both in all-singlet and SF channels, might be present within the solar spectrum range with $R_{1 \rightarrow 2} \sim 10^{14} \text{ s}^{-1}$, while $R_{2 \rightarrow 1}/R_{1 \rightarrow 2} \leq 10^{-2}$; it was estimated that $QE \simeq 1.2 - 1.6$. However, MEG strength in these SWCNTs was found to vary strongly with the excitation energy due to highly non-uniform density of states. In contrast, the MEG rate calculation done for (6,2) with Cl atoms adsorbed to the surface indicated that MEG efficiency in these systems could be enhanced by altering the low-energy electronic spectrum via, *e.g.*, surface functionalization [26].

Carrier multiplication and recombination without exciton effects and phonon-mediated relaxation was studied using coupled rate equations in coupled silicon nanocrystals in [27].

In this work we develop and apply a Boltzmann transport equation (BE) approach to study MEG in chiral SWCNTs including both exciton multiplication and recombination, *i.e.*, the Auger processes, and the phonon-mediated exciton relaxation. The Kadanoff-Baym-Keldysh, or NEGF, formalism - a generalization of DFT-based MBPT for a non-equilibrium state - allows one to use perturbation theory to calculate collision integrals in the transport equation for time evolution of a weakly non-equilibrium photoexcited state [28–30]. Notably, while BE coefficients can be computed to a given order in MBPT, BE itself is non-perturbative. We calculate QE for the (6,2) and (6,5) SWCNTs. This work aims to provide insights into dynamics of photoexcited SWCNTs and its dependence on the chirality, diameter and excitation energy.

The paper is organized as follows. Section II contains description of the methods and approximations used in this work. Section III contains description of the atomistic models used in this work and of the simulation details. Section IV contains discussion of the results obtained. Conclusions and Outlook are presented in Section V.

II. THEORETICAL METHODS AND APPROXIMATIONS

A. Electron Hamiltonian in the KS basis and Approximations

The the electron field operator $\psi_\alpha(\mathbf{x})$ and the annihilation operator of the i^{th} Kohn-Sham (KS) state $a_{i\alpha}$ are related via

$$\psi_\alpha(\mathbf{x}) = \sum_i \phi_{i\alpha}(\mathbf{x}) a_{i\alpha}, \quad (1)$$

where $\phi_{i\alpha}(\mathbf{x})$ is the i^{th} KS orbital, and α is the electron spin index [31, 32]. Here we only consider spin non-polarized states with $\phi_{i\uparrow} = \phi_{i\downarrow} \equiv \phi_i$; also $\{a_{i\alpha}, a_{j\beta}^\dagger\} = \delta_{ij}\delta_{\alpha\beta}$, $\{a_{i\alpha}, a_{j\beta}\} = 0$. Then, in terms of $a_{i\alpha}$, $a_{i\alpha}^\dagger$, the Hamiltonian of electrons in a CNT is (see, *e.g.*, [25, 26, 33].

$$H = \sum_{i\alpha} \epsilon_i a_{i\alpha}^\dagger a_{i\alpha} + H_C - H_V + H_{e-exciton}. \quad (2)$$

where $\epsilon_{i\uparrow} = \epsilon_{i\downarrow} \equiv \epsilon_i$ is the i^{th} KS energy eigenvalue. Typically, in a periodic structure $i = \{n, \mathbf{k}\}$, where n is the band number, \mathbf{k} is the lattice wavevector. However, for reasons explained in Section III here KS states are labeled by just integers. The second term is the (microscopic) Coulomb interaction operator

$$H_C = \frac{1}{2} \sum_{ijkl} \sum_{\alpha,\beta} V_{ijkl} a_{i\alpha}^\dagger a_{j\beta}^\dagger a_{k\beta} a_{l\alpha}, \quad V_{ijkl} = \int d\mathbf{x} d\mathbf{y} \phi_i^*(\mathbf{x}) \phi_j^*(\mathbf{y}) \frac{e^2}{|\mathbf{x} - \mathbf{y}|} \phi_k(\mathbf{y}) \phi_l(\mathbf{x}). \quad (3)$$

The H_V term prevents double-counting of electron interactions

$$H_V = \sum_{ij} a_{i\alpha}^\dagger \left(\int d\mathbf{x} d\mathbf{y} \phi_i^*(\mathbf{x}) V_{KS}(\mathbf{x}, \mathbf{y}) \phi_j(\mathbf{y}) \right) a_{j\alpha}, \quad (4)$$

where $V_{KS}(\mathbf{x}, \mathbf{y})$ is the KS potential consisting of the Hartree and exchange-correlation terms (see, *e.g.*, [34, 35]). Photon and electron-photon coupling terms are not directly relevant to this work and, so, are not shown, for brevity.

In this work we will consider singlet excitons only, leaving triplet exciton effects for future work. Before discussing the last term in the Hamiltonian (2) let us recall that in the Tamm-Dancoff approximation a spin-zero exciton state can be represented as [36, 37]

$$|\alpha\rangle_0 = B^{\alpha\dagger} |g.s.\rangle = \sum_{eh} \sum_{\sigma=\uparrow,\downarrow} \frac{1}{\sqrt{2}} \Psi_{eh}^\alpha a_{e\sigma}^\dagger a_{h\sigma} |g.s.\rangle, \quad (5)$$

where the index ranges are $e > HO$, $h \leq HO$, where HO is the highest occupied KS level, $LU = HO + 1$ is the lowest unoccupied KS level, and where $B^{\alpha\dagger}$, Ψ_{eh}^α are the singlet exciton creation operator and wavefunction, respectively. Then, the last term in the Hamiltonian (2) is

$$\begin{aligned} H_{e-exciton} = & \sum_{eh\alpha} \sum_{\sigma} \frac{1}{\sqrt{2}} ([\epsilon_{eh} - E^\alpha] \Psi_{eh}^\alpha a_{h\sigma} a_{e\sigma}^\dagger (B^\alpha + B^{\alpha\dagger}) + h.c.) + \\ & + \sum_{\alpha} E^\alpha B^{\alpha\dagger} B^\alpha, \quad \epsilon_{eh} = \epsilon_e - \epsilon_h, \end{aligned} \quad (6)$$

where E^α are the singlet exciton energies. The $H_{e-exciton}$ term can be seen as the result of re-summation of perturbative corrections to the propagating electron-hole state whereby exciton states emerge instead of electron-hole pairs (see, *e.g.*, [38, 39]); it describes coupling of excitons to electrons and holes, which allows systematic inclusion of excitons in the perturbative calculations [39–42]. See [26] for more details. To determine exciton wave functions and energies one solves the Bethe-Salpeter equation (BSE) [36, 37]. In the static screening approximation commonly used for semiconductor nanostructures (see, *e.g.*, [43–45]) the BSE is [44]

$$\begin{aligned} (\epsilon_{eh} - E^\alpha) \Psi_{eh}^\alpha + \sum_{e'h'} (K_{Coul} + K_{dir})(e, h; e', h') \Psi_{e'h'}^\alpha = 0, \\ K_{Coul} = \sum_{\mathbf{q} \neq 0} \frac{8\pi e^2 \rho_{eh}(\mathbf{q}) \rho_{e'h'}^*(\mathbf{q})}{V q^2}, \quad K_{dir} = -\frac{1}{V} \sum_{\mathbf{q} \neq 0} \frac{4\pi e^2 \rho_{ee'}(\mathbf{q}) \rho_{hh'}^*(\mathbf{q})}{q^2 - \Pi(0, -\mathbf{q}, \mathbf{q})}, \end{aligned} \quad (7)$$

where

$$\rho_{ji}(\mathbf{p}) = \sum_{\mathbf{k}} \phi_j^*(\mathbf{k} - \mathbf{p}) \phi_i(\mathbf{k}), \quad (8)$$

is the transitional density, and

$$\begin{aligned} \Pi(\omega, \mathbf{k}, \mathbf{p}) = & \frac{8\pi e^2}{V \hbar} \sum_{ij} \rho_{ij}(\mathbf{k}) \rho_{ji}(\mathbf{p}) \left(\frac{\theta_{-j} \theta_i}{\omega - \omega_{ij} + i\gamma} - \frac{\theta_j \theta_{-i}}{\omega - \omega_{ij} - i\gamma} \right), \\ \hbar \omega_{ij} = & \epsilon_{ij}, \quad \sum_i \theta_i = \sum_{i>HO}, \quad \sum_i \theta_{-i} = \sum_{i \leq HO}, \end{aligned} \quad (9)$$

is the RPA polarization insertion (see, *e.g.*, [31]).

A major screening approximation used in this work (see Eq. (7) and Eq. (22)) is that $\Pi(0, \mathbf{k}, \mathbf{p}) \simeq \Pi(0, -\mathbf{k}, \mathbf{k}) \delta_{\mathbf{k}, -\mathbf{p}}$ corresponding to $\Pi(0, \mathbf{x}, \mathbf{x}') \simeq \Pi(0, \mathbf{x} - \mathbf{x}')$, *i.e.*, to the uniform medium approximation. See [25, 26] for more details and discussion of applicability to SWCNTs.

Here, we have used hybrid Heyd-Scuseria-Ernzerhof (HSE06) exchange correlation functional in our DFT simulations [46, 47] as it has been successful in reproducing electronic gaps in various semiconductor nanostructures (*e.g.*, [35, 48, 49]). (See, however, [50].) Therefore, using the HSE06 functional is to substitute for GW corrections to the KS energies – the first step in the standard three-step procedure [36, 51]. So, single-particle energy levels and wave functions are approximated by the KS ϵ_i and $\phi_i(\mathbf{x})$ from the HSE06 DFT output. While inclusion of GW corrections would improve accuracy of our calculations, it is unlikely to alter our results and conclusions qualitatively.

Next, we describe how BE follows from the Keldysh MBPT which is the approach to the description of time evolution of a photoexcited state used in this work.

B. Boltzmann transport equation from Kadanoff-Baym-Keldysh formalism

Description of time evolution of a photoexcited nanoparticle should be comprehensive and, thus, include dynamics of electrons, phonons and, also, photons, if one aims to include absorption and recombination. For instance, to study MEG one needs to allow carrier multiplication to “compete” with the phonon-mediated relaxation, and, possibly, other processes, such as the energy and charge transfer.

Boltzmann transport equation (BE) is a suitable approach to this problem. The Kadanoff-Baym-Keldysh, or NEGF, formalism - a generalization of MBPT for non-equilibrium states - allows one to calculate collision integrals in the transport equation for time evolution of a weakly non-equilibrium photoexcited state [28–30]. As noted above, while BE collision integrals can be computed to a given order in MBPT, BE itself provides non-perturbative description.

Typically, a simple relaxation time approximation is used for the collision integral [30] (see, *e.g.*, [52] for a recent application). However, it is known that the equation of motion for the Keldysh propagator G^{-+} in the quasi-classical limit reduces to the transport equation [30]. This allows for systematic calculations of the collision integrals using Keldysh MBPT.

Let us consider correlation function $G_{\alpha}^{-+}(t_1, t_2) = \langle \mathcal{N} | B_{\alpha}^{\dagger}(t_2) B_{\alpha}(t_1) | \mathcal{N} \rangle$, where $|\mathcal{N}\rangle$ is some weakly non-equilibrium state, such as a photoexcited state at finite temperature, $B_{\alpha}(t)$ is the α^{th} exciton state Heisenberg operator. Note that G_{α}^{-+} is related to the density matrix.

The equation of motion for $G_{\alpha}^{-+}(t_1, t_2)$ is

$$\left(i\frac{d}{dt_1} - \frac{E_{\alpha}}{\hbar}\right) G_{\alpha}^{-+}(t_1, t_2) = \int dt_3 (\Sigma_{\alpha}^{--}(t_1, t_3)G_{\alpha}^{-+}(t_3, t_2) + \Sigma_{\alpha}^{-+}(t_1, t_3)G_{\alpha}^{++}(t_3, t_2)), \quad (10)$$

where Σ_{α}^{-+} , Σ_{α}^{--} , G_{α}^{++} are the Keldysh self-energies and correlators, respectively. BE obtains when the slow $t = (t_1 + t_2)/2$ and fast (intrinsic) $t_0 = t_1 - t_2$ times are introduced (see paragraph 95 of [30] for details). It describes slow time-evolution of a weakly non-equilibrium state. For instance, the $t_1 \rightarrow t_2$ components of G_{α}^{-+} are the exciton occupation numbers: $n_{\alpha}(t) = G_{\alpha}^{-+}(t, t)$. It is the set of $n_{\alpha}(t)$ that describes the non-equilibrium state $|\mathcal{N}\rangle$. Then BE for the (slow) time evolution of a photo-excited state is

$$\dot{n}_{\alpha} = i\Sigma_{\alpha}^{-+}(n; \omega_{\alpha})(1 + n_{\alpha}) - i\Sigma_{\alpha}^{+-}(n; \omega_{\alpha})n_{\alpha}, \quad \omega_{\alpha} = \frac{E_{\alpha}}{\hbar}, \quad (11)$$

where Σ_{α}^{-+} , Σ_{α}^{+-} are the leading Keldysh exciton self-energies, which depend on the slowly varying occupation numbers. Different contributions to the self-energies that correspond to different processes will be discussed below. Note the r.h.s. of Eq. 11 has the expected “gain” - “loss” term structure. The approach is applicable if $\dot{n}_{\alpha}(t) \ll \omega_{\alpha}$, which is the quasi-classicality condition in this case. Solving the system of equations (11) with the initial condition $n_{\alpha}(t=0) \neq 0$ for $\hbar\omega_{\alpha} = \hbar\omega$, where the excitation energy $\hbar\omega$ corresponds to, *e.g.*, an absorption peak, will yield description of relaxation in a photo-excited nanoparticle.

As mentioned above, here we aim to describe dynamics of a photoexcited SWCNT including electron-hole bound state (exciton) effects and taking into account (I) phonon-mediated relaxation, *i.e.*, the non-adiabatic processes; (II) exciton-to-bi-exciton decay and bi-exciton recombination, *i.e.*, inverse and direct Auger processes. Collision integrals for these two processes will be described in the next two sub-sections.

Then, in order to calculate internal QE one

1. populates exciton with energy E ; the initial state is $n_i(0) = n_{in}\delta_{i\alpha}$, $E_{\alpha} = E$,
2. solves BE including a. phonon emission and absorption terms, b. exciton-to-bi-exciton decay and recombination,
3. adds up the occupation numbers of excitons generated after the occupancies have plateaued as $t \rightarrow \infty$. (Recall that recombination occurring on a much longer time scale is not included here.) After the initial state averaging,

$$QE(E) = \frac{\sum_{\alpha} n_{\alpha}}{n_{in}}. \quad (12)$$

C. Electron-Phonon Interaction

In order to include phonon terms and the electron-phonon coupling Hamiltonian (2) is augmented with

$$H_N = \sum_{I=1}^{N_{ion}} \frac{P_I^2}{2M_I} + V_{NN}, \quad V_{NN} \simeq \frac{1}{2} \sum_{I \neq J} \frac{Z_I Z_J e^2}{|\mathbf{R}_I - \mathbf{R}_J|}, \quad (13)$$

where \mathbf{P}_I , \mathbf{R}_I , M_I , Z_I are the I^{th} ion momentum, position, mass, and effective charge – number of valence electrons, respectively; \mathbf{P}_I , \mathbf{R}_I are the ion momentum and position operators, respectively, $I = 1, \dots, N_{ion}$. One sets $\mathbf{R}_I = \mathbf{R}_I^0 + \mathbf{r}_I$, where the equilibrium ion positions \mathbf{R}_I^0 corresponding to the energy minimum have been found by, *e.g.*, the DFT geometry relaxation procedure, and \mathbf{r}_I are small oscillations about equilibrium. This leads to the following phonon and electron-phonon terms in the Hamiltonian (see, *e.g.*, [53, 54])

$$\delta H_{e-ph} = \sum_{\nu=1}^{3N_{ion}-6} \hbar \omega_{\nu} \left(c_{\nu}^{\dagger} c_{\nu} + \frac{1}{2} \right) + \sum_{ij\nu\sigma} g_{ij}^{\nu} a_{i\sigma}^{\dagger} a_{j\sigma} (c_{\nu}^{\dagger} + c_{\nu}), \quad (14)$$

where c_{ν} is the phonon annihilation operator, and the electron-phonon couplings are [54]

$$g_{ij}^{\nu} = \sum_{I=1}^{N_i} \frac{4\pi i Z_I e^2}{V} \sqrt{\frac{\hbar}{2\omega_{\nu} M_I}} \sum_{\mathbf{p}} \frac{\rho_{ji}^*(\mathbf{p}) (\mathbf{p} \cdot \mathbf{U}_I^{\nu}) e^{-i\mathbf{p} \cdot \mathbf{R}_I}}{p^2 - \Pi(0, -\mathbf{p}, \mathbf{p})}. \quad (15)$$

This is similar to the frozen photon approximation [55, 56]. Our approach is applicable to the systems where atoms undergo small oscillations about their equilibrium positions; the electronic states are approximated using equilibrium atomic positions \mathbf{R}_I^0 . Normal frequencies, ω_{ν} , and mode decompositions, \mathbf{U}_I^{ν} , are calculated using DFT software, such as VASP. The pseudopotential $v(\mathbf{x}, \mathbf{R}_I)$ felt by the valence electrons is approximated here by the Coulomb interaction, which is also (approximately) screened [31].

The $\mathcal{O}(r_I^2)$ contribution to δH_{e-ph} (see, *e.g.*, [57]) is neglected since it does not contribute to the exciton-phonon Keldysh couplings at the leading one-phonon level. More generally, the $\mathcal{O}(r_I^2)$ term's contribution is suppressed due to screening of $v(\mathbf{x}, \mathbf{R}_I)$ [31, 58].

So, in order to describe phonon-mediated relaxation in a nanoparticle one includes electron-phonon interactions described above in Eqs. (14,15). The corresponding Feynman diagrams are shown in Fig. 1. In SWCNTs sub-gaps in the electronic energy spectrum are sizable enough for the two-phonon processes (Fig. 1, (b)) to be relevant. With the one-

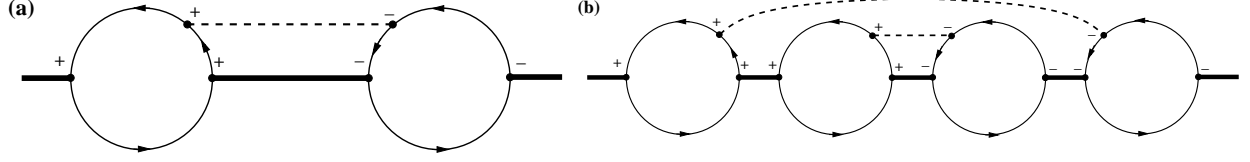


FIG. 1: Typical Feynman diagrams for the Σ^{+-} describing exciton-phonon coupling. Shown in (a) and (b) are the one- and two-phonon processes, respectively. Thin solid lines stand for the KS state propagators, thick solid lines depict excitons, dashed lines – phonons. The $-+$ contributions obtain when $+$ and $-$ are interchanged.

and two-phonon processes included the BE is

$$\begin{aligned} \dot{n}_\alpha = & \sum_{\alpha\mu} (G_1)_{\alpha\beta}^\mu (n_\beta n_\mu - n_\alpha (n_\beta + n_\mu + 1)) \delta(\omega_\alpha - \omega_\beta - \omega_\mu) + \\ & + \sum_{\alpha\mu\nu} (G_2)_{\alpha\beta}^{\mu\nu} (n_\mu n_\nu (n_\beta - n_\alpha) - n_\alpha (n_\beta + 1) (n_\mu + n_\nu) - n_\alpha (n_\beta + 1)) \times \\ & \times \delta(\omega_\alpha - \omega_\beta - \omega_\mu - \omega_\nu) - \{\alpha \leftrightarrow \beta\}, \text{ where} \end{aligned} \quad (16)$$

$$n_\nu \simeq \left(\exp \left[\frac{\hbar\omega_\nu}{k_B T} \right] - 1 \right)^{-1}, \quad (17)$$

and

$$(G_1)_{\alpha\beta}^\mu \simeq \frac{2\pi}{\hbar^2} \left(\left| \sum_{ijk} \theta_{-i} \theta_j \theta_k g_{jk}^\mu (\Psi_{ji}^\alpha)^* \Psi_{ki}^\beta \right|^2 + \left| \sum_{ijk} \theta_i \theta_{-j} \theta_{-k} g_{jk}^\mu \Psi_{ij}^\alpha (\Psi_{ik}^\beta)^* \right|^2 \right), \quad (18)$$

where $(G_1)_{\alpha\beta}^\mu$ are the dominant terms of the effective exciton-phonon couplings, T is the temperature. Also,

$$\begin{aligned} (G_2)_{\alpha\beta}^{\mu\nu} \simeq & \frac{2\pi}{\hbar^4} \left| \sum_{pkqjli} \sum_{\sigma} \frac{1}{\omega_\alpha + \omega_\mu - \omega_\sigma + i\delta} (c_{pp} + c_{hh} + c_{ph} + c_{hp}) \right|^2, \\ c_{pp} = & g_{pk}^\mu g_{qj}^\nu \frac{\theta_{-k} \theta_l \theta_{-p} (\Psi_{lk}^\alpha)^* \Psi_{lp}^\sigma (\omega_{lp} - \omega_\sigma)}{\omega_{lp} - \omega_\alpha - \omega_\mu - i\delta} \frac{\theta_i \theta_{-j} \theta_{-q} (\Psi_{ij}^\sigma)^* (\omega_{ij} - \omega_\sigma) \Psi_{iq}^\beta}{\omega_{ij} - \omega_\alpha - \omega_\mu - i\delta}, \\ c_{hh} = & g_{pj}^\mu g_{ql}^\nu \frac{\theta_{-i} \theta_j \theta_p \Psi_{ji}^\alpha (\Psi_{pi}^\sigma)^* (\omega_{pi} - \omega_\sigma)}{\omega_\alpha + \omega_\mu - \omega_{pi} + i\delta} \frac{\theta_{-k} \theta_l \theta_q \Psi_{lk}^\sigma (\omega_{lk} - \omega_\sigma) (\Psi_{qk}^\beta)^*}{\omega_\alpha + \omega_\mu - \omega_{lk} + i\delta}, \\ c_{hp} = & g_{jq}^\nu g_{pk}^\mu \frac{\theta_k \theta_{-l} \theta_p \Psi_{kl}^\alpha (\Psi_{pl}^\sigma)^* (\omega_{pl} - \omega_\sigma)}{\omega_\alpha + \omega_\mu - \omega_{pl} + i\delta} \frac{\theta_i \theta_{-j} \theta_{-q} \Psi_{ij}^\sigma (\omega_{ij} - \omega_\sigma) (\Psi_{iq}^\beta)^*}{\omega_{ij} - \omega_\alpha - \omega_\mu - i\delta}, \\ c_{ph} = & g_{kp}^\mu g_{qj}^\nu \frac{\theta_{-k} \theta_l \theta_{-p} \Psi_{lk}^\alpha (\Psi_{lp}^\sigma)^* (\omega_{lp} - \omega_\sigma)}{\omega_{lp} - \omega_\alpha - \omega_\mu - i\delta} \frac{\theta_{-i} \theta_j \theta_q \Psi_{ji}^\sigma (\omega_{ji} - \omega_\sigma) (\Psi_{qi}^\beta)^*}{\omega_\alpha - \omega_{ji} + \omega_\mu + i\delta}, \end{aligned} \quad (19)$$

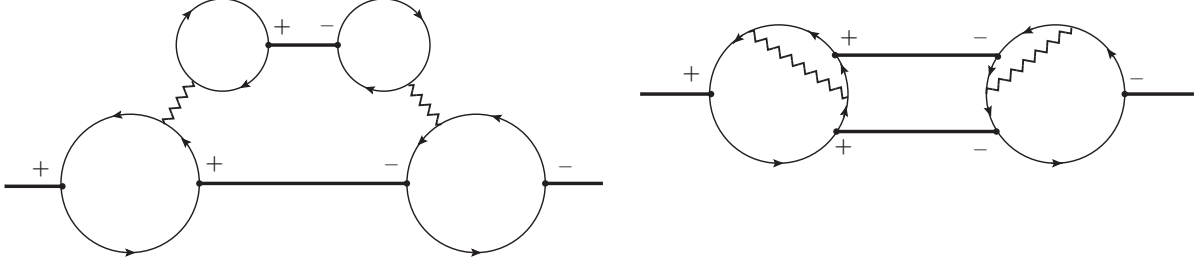


FIG. 2: Exciton self-energy Feynman diagrams relevant for the exciton \rightarrow bi-exciton and bi-exciton \rightarrow exciton processes. Thin solid lines stand for the KS state propagators, thick solid lines depict excitons, zigzag lined – screened Coulomb potential. The diagrams on the left and the right correspond to the exchange and direct channels, respectively. Not shown for brevity are the similar diagrams with all the Fermion arrows reversed and with + and - interchanged.

where δ is the small width parameter set here to the temperature scale 25 meV . Both phonon emission and absorption from the thermal bath by either the electron or the hole within the exciton are included in Eq. (16). The two-phonon processes where one phonon is emitted and the other one is absorbed are not included in Eq. (16), for technical simplicity. Also, in this perturbative approach phonon occupation numbers are approximated by their equilibrium values (see Eq. (17)), which is another technical simplification.

In the above and in the following expressions only the terms leading in the ratio of the typical exciton binding energy to the gap ($\epsilon_{\text{binding}}/E_g$) < 1 are shown, for brevity. But full expressions have been included in the actual calculations.

D. MEG terms

Transport equations that describe exciton-to-biexciton decay and biexciton-to-exciton recombination are

$$\begin{aligned} \frac{dn_\gamma}{dt} &= \sum_{\alpha\beta} R_{\alpha\beta}^\gamma (n_\alpha n_\beta - n_\gamma (n_\alpha + n_\beta + 1)) \delta(\omega_\alpha + \omega_\beta - \omega_\gamma), \\ n_\alpha \frac{dn_\beta}{dt} + n_\beta \frac{dn_\alpha}{dt} &= - \sum_\gamma R_{\alpha\beta}^\gamma (n_\alpha n_\beta - n_\gamma (n_\alpha + n_\beta + 1)) \delta(\omega_\alpha + \omega_\beta - \omega_\gamma), \end{aligned} \quad (20)$$

where $R_{\alpha\beta}^\gamma$ are the rates from the MEG contributions to Σ_α^{-+} , Σ_α^{+-} shown in Fig. 2. In (20) the first equation describes the I.I. process where exciton γ decays into excitons α and β ; the second – inverse recombination process (direct Auger). The leading order rate expressions

are (α, β, γ subscripts are omitted for brevity) [25]

$$\begin{aligned}
R_{\alpha\beta}^{\gamma} &= \left(R^p + R^h + \tilde{R}^p + \tilde{R}^h \right) \delta(\omega_{\gamma} - \omega_{\alpha} - \omega_{\beta}), \\
R^p &= 2 \frac{2\pi}{\hbar^2} \left| \sum_{ijkln} W_{jlnk} \theta_l \theta_{-n} (\Psi_{ln}^{\beta})^* \theta_i \theta_{-j} \theta_{-k} \Psi_{ij}^{\gamma} (\Psi_{ik}^{\alpha})^* \right|^2, \\
R^h &= 2 \frac{2\pi}{\hbar^2} \left| \sum_{ijkln} W_{jlnk} \theta_{-l} \theta_n \Psi_{nl}^{\beta} \theta_{-i} \theta_j \theta_k (\Psi_{ji}^{\gamma})^* \Psi_{ki}^{\alpha} \right|^2.
\end{aligned} \tag{21}$$

The expressions for \tilde{R}^h and \tilde{R}^p are the same as the ones for R^h , R^p with W_{jlnk} replaced by $W_{jlk n}$ and divided by 2. In the above

$$W_{jlnk} = \sum_{\mathbf{q} \neq 0} \frac{4\pi e^2}{V} \frac{\rho_{kj}^*(\mathbf{q}) \rho_{ln}(\mathbf{q})}{(q^2 - \Pi(0, -\mathbf{q}, \mathbf{q}))} \tag{22}$$

is the (approximate) screened Coulomb matrix element.

Strictly speaking, here we are working to the second order in the screened Coulomb interaction. This refers to the electron \rightarrow trion, hole \rightarrow trion sub-processes in Fig. 2, *i.e.*, the trion is created in the course of a single Coulomb interaction. However, as discussed above, the electron-hole interactions that form the excitons are included to all orders. Also, in this work a biexciton state is approximated by a pair of non-interacting excitons.

III. COMPUTATIONAL DETAILS

The optimized SWCNT geometries, KS orbitals and energy eigenvalues have been obtained using the *ab initio* total energy and molecular dynamics program VASP (Vienna *ab initio* simulation program) with the hybrid Heyd-Scuseria-Ernzerhof (HSE06) exchange correlation functional [46, 47] using the projector augmented-wave (PAW) pseudopotentials [59, 60].

Applying conjugated gradient method for atomic position relaxation the structures were relaxed until residual forces on the ions were no greater than 0.05 eV/Å. The momentum cutoff defined by

$$\frac{\hbar^2 k^2}{2m} \leq \mathcal{E}_{max}, \tag{23}$$

where m is the electron mass, was chosen at $\mathcal{E}_{max} = 400$ eV. The energy cutoffs determined by the number of KS orbitals included in the simulations were chosen so that

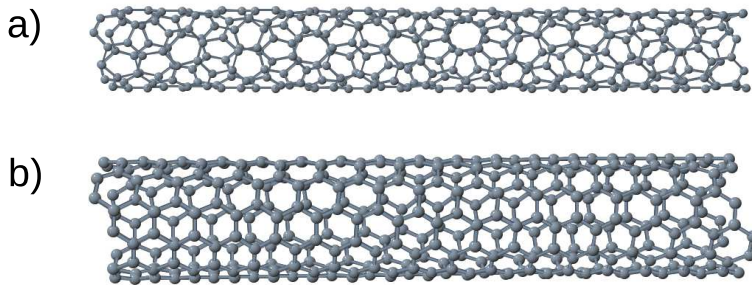


FIG. 3: Atomistic models of chiral SWCNTs. Shown in a) is SWCNT (6,2). Three unit cells have been included in the simulations. In b) is SWCNT (6,5). Only one unit cell is included due to computational cost restrictions.

$\epsilon_{i_{max}} - \epsilon_{HO} \simeq \epsilon_{LU} - \epsilon_{i_{min}} \geq 3 \text{ eV}$, where i_{max} , i_{min} are the highest and the lowest KS labels included in simulations. SWCNT atomistic models were placed in the finite volume simulation boxes with periodic boundary conditions. In the axial direction the box size was chosen to accommodate an integer number of unit cells. In the other two directions the SWCNTs have been kept separated by about 1 *nm* of vacuum surface-to-surface which excluded spurious interactions between their periodic images. As discussed in [25], we have found reasonably small (about 10%) variation in the single particle energies over the Brillouin zone when three unit cells were included in the DFT simulations [25]. Therefore, in (6,2) simulations have been done at the Γ point including three unit cells. In our approximation lattice momenta of the KS states, which are suppressed by the reduced Brillouin zone size, have been neglected. Due to high computational cost, for (6,5) SWCNT only one unit cell was included. However, we checked that this size-reduced model reproduced the absorption spectrum features with the accuracy similar to other SWCNTs [26]. As explained before in [25], the rationale for including multiple unit cells instead of the Brillouin zone sampling in the DFT simulations is that surfaces of these SWCNTs are to be functionalized. Inclusion of several unit cells keeps the concentration of surface dopants reasonably low. The atomistic models of the optimized nanotubes are shown in Fig. (3).

In this work all the DFT simulations have been done in a vacuum which is to approximate properties of these SWCNTs dispersed in a non-polar solvent.

IV. RESULTS AND DISCUSSION

First, we have simulated relaxation of an energetic exciton state corresponding to the absorption peak E_{22} including electron-phonon interactions only. The results are shown

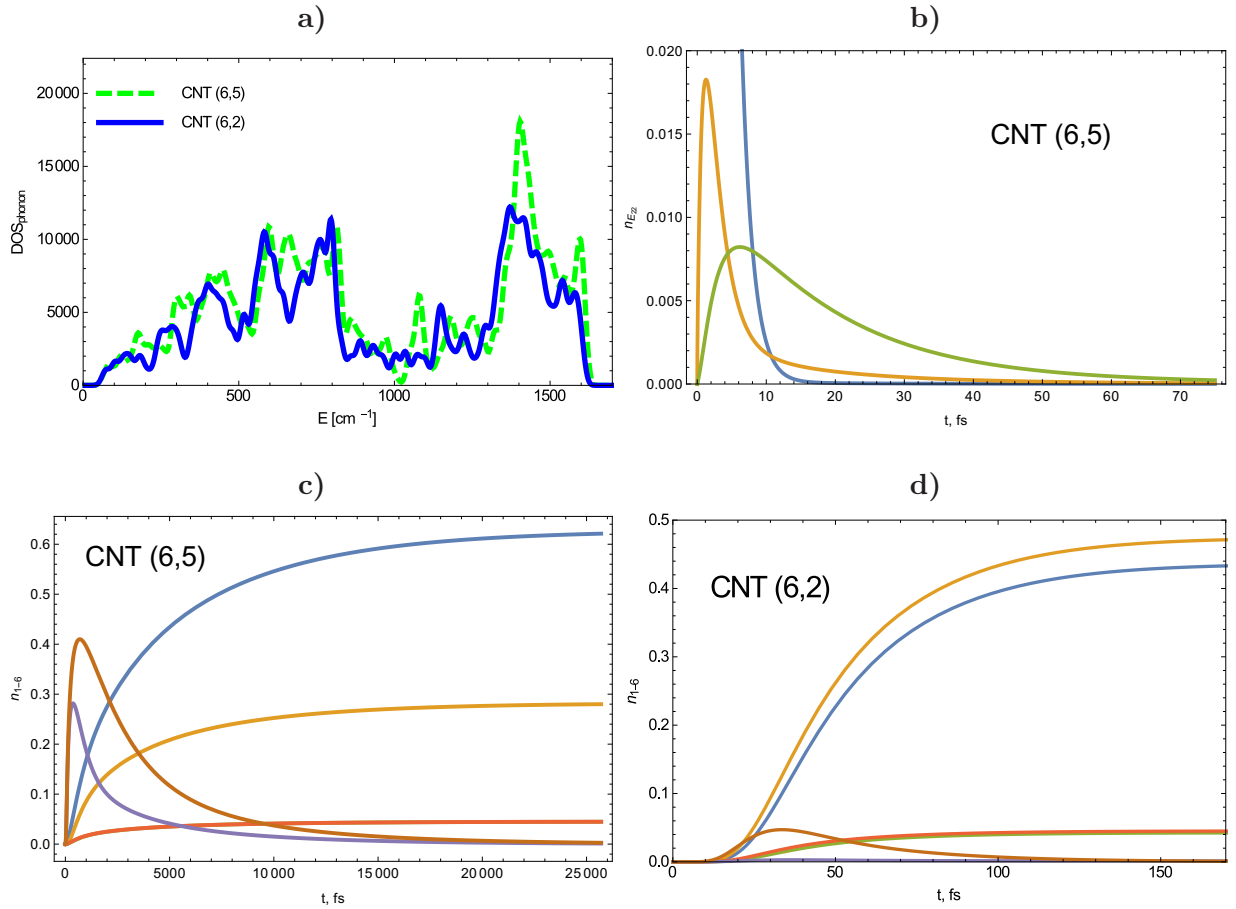


FIG. 4: Phonon DOSs for the two CNTs are shown in a). Shown in b) are the occupation numbers of the exciton states corresponding to the E_{22} peak energy in CNT (6,5). In c) and d) are the few low-energy exciton occupancies after excitation at the E_{22} peak energy in (6,5) and (6,2), respectively.

in Fig. (4). Phonon spectra for CNTs (6,2) and (6,5) computed using VASP are in Fig. (4), a). Shown in Fig. (4), b) are the occupancies of the E_{22} peak exciton states in CNT (6,5). As expected, the initial excitation is cascading down in energy. Intermediate states are being excited and subsequently decay in the course of the relaxation. An exponential fit to the predicted $n_{E_{22}}(t)$ curve has yielded decay constant $\tau_{22} = 16.7 \text{ fs}$. The available experimental results are for (6,5) in the aqueous solution where $\tau_{22} = 120 \text{ fs}$ was reported [61]. For SWCNTs of unspecified chiralities immersed in polyethylene glycol and in polymethylmethacrylate $\tau_{22} \simeq 40 \text{ fs}$ was reported [62, 63]. So, while direct comparison is not possible at this time, it is likely that our prediction for τ_{22} is underestimated. This is as expected and is in line with other predictions of our approach which tends to overestimate strength of couplings. Overall, this confirms applicability of our method for semi-quantitative description

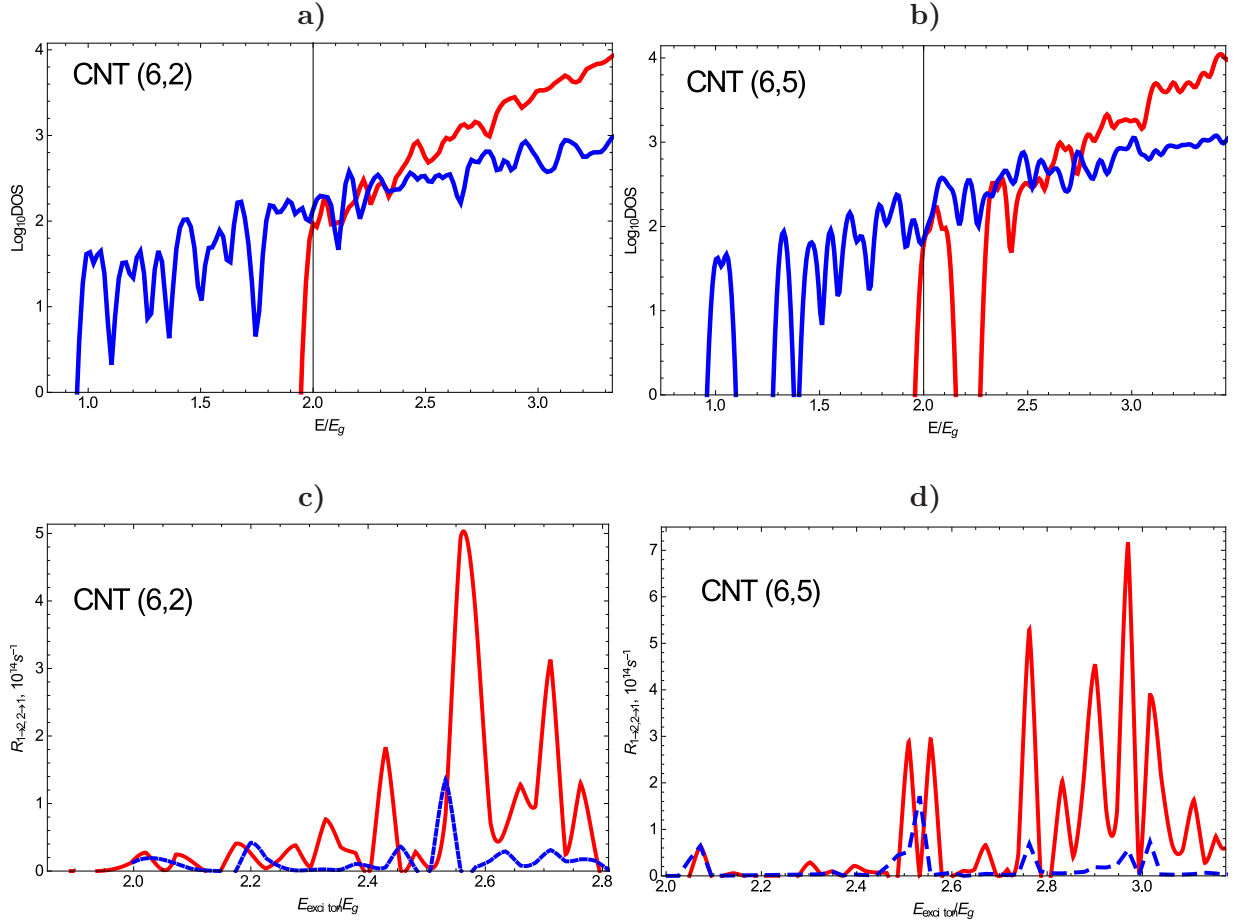


FIG. 5: Exciton and bi-exciton DOSs for the CNT (6,2) ($E_g = 0.98 \text{ eV}$) and CNT (6,5) ($E_g = 1.09 \text{ eV}$) are shown in a) and b), respectively; in c) and d) are the exciton-to-biexciton, bi-exciton-to-exciton rates $R_{1 \rightarrow 2}$, $R_{2 \rightarrow 1}$ in CNT (6,2) and (6,5), respectively. *Note that recombination rate magnitude – the dashed curves in c) and d) – has been multiplied by 100.*

of photoexcited chiral SWCNT dynamics.

Shown in Fig. (4), c) and d) are the few low-energy exciton occupancies resulting from the excitation at the E_{22} peak energy for (6,5) and (6,2), respectively. The excitation goes through several transient states before forming a terminal steady state where only few low-energy levels are occupied. In (6,2) the relaxation time from the E_{22} excitation is about 100 fs (Fig. (4), d)), while in (6,5) the E_{22} relaxation time is predicted to be two orders of magnitude longer (Fig. (4), c)). The results suggest that relaxation rates in CNTs strongly depend on the diameter and chirality.

Next, we augmented the system of equations for $n_\alpha(t)$ with the MEG terms. Now as the excitation is cascading down the energy levels by emitting and absorbing phonons, it can, also, undergo an exciton \rightarrow bi-exciton decay. Conversely, the bi-exciton state can recombine

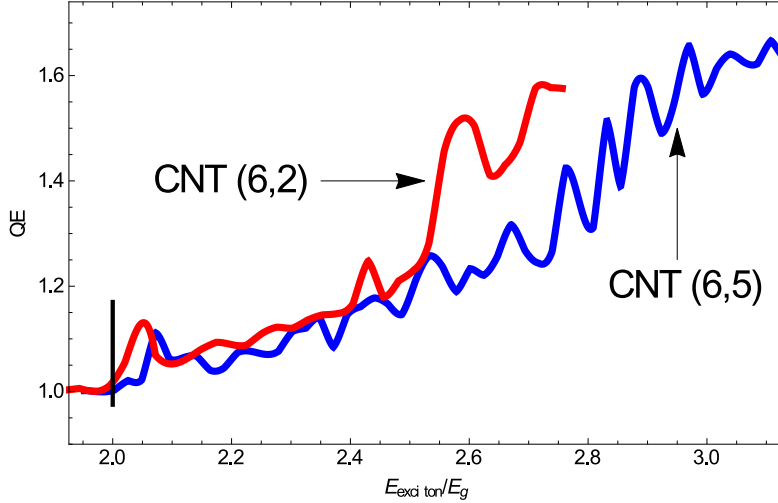


FIG. 6: The QEs for the CNT (6,2) and (6,5) *vs.* E/E_g , where $E_g = 0.98$ eV for (6,2) and for (6,5) $E_g = 1.09$ eV. Vertical dash indicates $2E_g^{BSE}$ threshold.

into a single high-energy exciton. For completeness, the exciton and bi-exciton spectra, as well as the exciton→bi-exciton rates from [25] and [26] are shown in Fig. 5. These results suggest that MEG strength in SWCNTs is likely to be determined by an intricate interplay between the Auger processes and phonon-mediated relaxation. For instance, just above the $2E_g$ threshold there are energy ranges where bi-exciton DOS is lower the DOS of single excitons (Fig. 5), a) and b)). Counterintuitively enough, the faster phonon-mediated relaxation will carry the excitation through these energy ranges the smaller fraction of bi-excitons will be able to recombine, thus enhancing MEG. Also, we note that for efficient MEG it is crucial to have non-zero $R_{1\rightarrow2}$ just above the $2E_g$ threshold.

Using the QE procedure outlined in Section II B we computed QE for the CNTs (6,2) and (6,5) as a function of the excitation energy. Our results are shown in Fig. 6. We predict efficient solar range MEG in both of these systems which starts at the threshold and reaches ~ 1.6 at about $3E_g$.

As already mentioned above, MEG in CNT (6,5) has been studied experimentally in [14]. QE was measured for two excitation energies: for $E = 2.5E_g^{opt}$ $QE = 1.1$ was reported, while our prediction is $QE \simeq 1.2$; for $E = 3E_g^{opt}$ $QE = 1.3$ *vs.* $QE \simeq 1.6$, which is our prediction. The ways to improve accuracy of our method are discussed in Section V.

V. CONCLUSIONS AND OUTLOOK

We have used Kadanoff-Baym-Keldysh, or NEGF, technique of MBPT to develop a comprehensive DFT-based description of time evolution of a photoexcited SWCNT. The approach is based on the Boltzmann transport equation for time evolution of a weakly non-equilibrium photoexcited state in the quasi-classical limit with collision integrals calculated from the DFT-based Keldysh MBPT. We have been working to the second order in the RPA-screened Coulomb interaction and including electron-hole bound state effects for which we had to solve BSE.

This method has been used to study MEG in the chiral SWCNTs, using (6,2) and (6,5) as examples. In particular, we calculated predictions for the internal QE as a function of the excitation energy. Our calculations suggest that chiral SWCNTs may have efficient MEG within the solar spectrum range (see Fig. 6).

In the pristine SWCNTs the MEG rates vary strongly with the excitation energy. In contrast, using *Cl*-decorated (6,2) SWCNT as an example it has been found that surface functionalization significantly alters low-energy spectrum in a SWCNT [26]. Also, in the doped case, the MEG rate is not only greater in magnitude, but also is a much smoother function of the excitation energy. QE calculations for the doped SWCNTs and for different chiral SWCNTs are in progress.

As described above, several simplifying approximations had to be utilized in order to be able to calculate properties of these SWCNTs. Previously, we checked have that our predictions for the absorption spectra were in a reasonable agreement with the experimental data with the error less then 13% for E_{11} and E_{22} peak energies for the (6,2), (6,5) and (10,5) nanotubes. As discussed in Section IV, in this work we compared our predictions for the phonon-mediated relaxation and for $QE(E)$ to the available experimental results for CNT (6,5). The comparison indicated that our current method is valid for SWCNTs at the semi-quantitative level. However, accuracy can be improved in several ways. For instance, static interaction approximation $\Pi(\omega, \mathbf{k}, \mathbf{p}) = \Pi(0, \mathbf{k}, \mathbf{p})$ is reasonably accurate when employed in the BSE. But in the impact ionization process the typical energy exchange is of order of the gap and, so, screening should be treated as dynamical. This is likely to enhanced screening (see Eq. (9) for $\omega \simeq E_g$) which could help alleviate the overbinding issue. Implementation of this is technically challenging and is left to future work. A straightforward improvement

is to include *GW* single particle energy corrections, which then can be easily incorporated in the rate expressions. It is likely to blue-shift the rate curves by a fraction of eV without significant changes to the overall shape. Another natural but technically challenging step is to use full RPA interaction $W(\omega, \mathbf{k}, \mathbf{p})$ rather than $W(0, -\mathbf{k}, \mathbf{k})$.

However, none of these corrections are likely to change the main results and conclusions of this work, while drastically increasing computational cost.

VI. ACKNOWLEDGMENTS

Authors acknowledge financial support from the NSF grant CHE-1413614. S.K. acknowledges partial support of the Alfred P. Sloan Research Fellowship BR2014-073 and NDSU Advance FORWARD program sponsored by NSF HRD-0811239 and EPS-0814442. The authors acknowledge the use of computational resources at the Center for Computationally Assisted Science and Technology (CCAST) at North Dakota State University and the National Energy Research Scientific Computing Center (NERSC) allocation award 86678, supported by the Office of Science of the DOE under contract No. DE-AC02-05CH11231.

-
- [1] W. Shockley and H. Queisser, J. Appl. Phys. **32**, 510 (1961).
 - [2] R. J. Ellingson, M. C. Beard, J. C. Johnson, P. R. Yu, O. I. Micic, A. J. Nozik, A. Shabaev, and A. L. Efros, Nano Letters **5**, 865 (2005).
 - [3] A. J. Nozik, Physica E: Low-dimensional Systems and Nanostructures **14**, 115 (2002).
 - [4] W. D. A. M. de Boer, E. M. L. D. de Jong, D. Timmerman, T. Gregorkiewicz, H. Zhang, W. J. Buma, A. N. Poddubny, A. A. Prokofiev, and I. N. Yassievich, Phys. Rev. B **88**, 155304 (2013).
 - [5] J. Stewart, L. Padilha, W. Bae, W. Koh, J. Pietryga, and V. Klimov, The Journal of Physical Chemistry Letters **4**, 2061 (2013).
 - [6] J. Bude and K. Hess, J. Appl. Phys. **72**, 3554 (1992).
 - [7] H. K. Jung, K. Taniguchi, and C. Hamaguchi, J. Appl. Phys. **79**, 2473 (1996).
 - [8] D. Harrison, R. A. Abram, and S. Brand, J. Appl. Phys. **85**, 8186 (1999).
 - [9] A. Nozik, Annual Review of Physical Chemistry **52**, 193 (2001).

- [10] R. Ellingson, M. Beard, J. Johnson, P. Yu, O. Micic, A. Nozik, A. Shabaev, and A. Efros, Nano Letters **5**, 865 (2005).
- [11] J. McGuire, M. Sykora, J. Joo, J. Pietryga, and V. Klimov, Nano Letters **10**, 2049 (2010).
- [12] N. M. Gabor, Accounts of Chemical Research **46**, 1348 (2013).
- [13] O. Semonin, J. Luther, S. Choi, H.-Y. Chen, J. Gao, A. J. Nozik, and M. C. Beard, Science **334**, 1530 (2011).
- [14] S. Wang, M. Khafizov, X. Tu, M. Zheng, and T. Krauss, Nano Letters **10**, 2381 (2010).
- [15] M. L. Bohm, T. C. Jellicoe, M. Tabachnyk, N. J. L. K. Davis, F. Wisnivesky-Rocca-Rivarola, C. Ducati, B. Ehrler, A. A. Bakulin, and N. C. Greenham, Nano Letters **15**, 7987 (2015).
- [16] M. L. Bohm, M. Tabachnyk, F. Wisnivesky-Rocca-Rivarola, T. C. Jellicoe, C. Ducati, B. Ehrler, and N. C. Greenham, Nature Communications **6**, 8259 (2015).
- [17] S. Saeed, P. de Weerd, C. Stallinga, F. Spoor, A. Houtepen, L. Siebbeles, and T. Gregorkiewicz, Light: Science and Applications **4**, 672 (2015).
- [18] M. T. Trinh, R. Limpens, W. de Boer, J. Schins, L. Siebbeles, and T. Gregorkiewicz, Nature Photonics **6**, 316 (2012).
- [19] N. Gabor, Z. Zhong, K. Bosnick, J. Park, and P. McEuen, Science **325**, 1367 (2009).
- [20] V. Perebeinos and P. Avouris, Phys. Rev. B **74**, 121410 (2006).
- [21] S. Konabe and S. Okada, Phys. Rev. Lett. **108**, 227401 (2012).
- [22] K. Velizhanin and A. Piryatinski, Phys. Rev. Lett. **106**, 207401 (2011).
- [23] K. A. Velizhanin and A. Piryatinski, Phys. Rev. B **86**, 165319 (2012).
- [24] S. Kilina, D. Kilin, and S. Tretiak, Chemical Reviews **115**, 5929 (2015).
- [25] A. Kryjevski, B. Gifford, S. Kilina, and D. Kilin, The Journal of Chemical Physics **145**, 154112 (2016).
- [26] A. Kryjevski, D. Mihaylov, B. Gifford, and D. Kilin, The Journal of Chemical Physics **147**, 000000 (2017).
- [27] I. Marri, M. Govoni, and S. Ossicini, Journal of the American Chemical Society **136**, 13257 (2014).
- [28] L. Kadanoff and G. Baym, *Quantum Statistical Mechanics* (W.A. Benjamin Inc., New York, 1962).
- [29] L. V. Keldysh, Zh. Eksp. Teor. Fiz. **47**, 1515 (1964), [Sov. Phys. JETP **20**, 1018(1965)].
- [30] E. M. Lifshitz and L. P. Pitaevskii, *Physical Kinetics* (Pergamon Press, New York, 1981), 1st

ed.

- [31] A. L. Fetter and J. Walecka, *Quantum Theory of Many-Particle Systems* (McGraw-Hill, New York, 1971).
- [32] G. Mahan, *Many-Particle Physics* (Plenum, New York, N.Y., 1993), 2nd ed.
- [33] A. Kryjevski and D. Kilin, *Molecular Physics* **112**, 430 (2014).
- [34] G. Onida, L. Reining, and A. Rubio, *Rev. Mod. Phys.* **74**, 601 (2002).
- [35] S. Kümmel and L. Kronik, *Rev. Mod. Phys.* **80**, 3 (2008).
- [36] M. Rohlfing and S. Louie, *Phys. Rev. B* **62**, 4927 (2000).
- [37] G. Strinati, *Phys. Rev. B* **29**, 5718 (1984).
- [38] V. Berestetskii, E. Lifshitz, and L. Pitaevskii, *Quantum Electrodynamics* (Oxford, U.K.: Pergamon Press, 1979).
- [39] S. Beane, P. Bedaque, W. Haxton, D. Phillips, and M. Savage, Shifman, M. (ed.): *At the frontier of particle physics* **1**, 133 (2000).
- [40] C. Spataru, S. Ismail-Beigi, L. Benedict, and S. Louie, *Phys. Rev. Lett.* **92**, 077402 (2004).
- [41] V. Perebeinos, J. Tersoff, and P. Avouris, *Phys. Rev. Lett.* **92**, 257402 (2004).
- [42] C. Spataru, S. Ismail-Beigi, R. Capaz, and S. Louie, *Phys. Rev. Lett.* **95**, 247402 (2005).
- [43] S. Ögüt, R. Burdick, Y. Saad, and J. Chelikowsky, *Phys. Rev. Lett.* **90**, 127401 (2003).
- [44] L. Benedict, A. Puzder, A. Williamson, J. Grossman, G. Galli, J. Klepeis, J.-Y. Raty, and O. Pankratov, *Phys. Rev. B* **68**, 085310 (2003).
- [45] H. Wilson, D. Lu, F. Gygi, and G. Galli, *Phys. Rev. B* **79**, 245106 (2009).
- [46] O. Vydrov, J. Heyd, A. Krukau, and G. Scuseria, *The Journal of Chemical Physics* **125**, 074106 (2006).
- [47] J. Heyd, G. Scuseria, and M. Ernzerhof, *The Journal of Chemical Physics* **124**, 219906 (2006).
- [48] J. Muscat, A. Wander, and N. Harrison, *Chemical Physics Letters* **342**, 397 (2001).
- [49] M. Govoni and G. Galli, *Journal of Chemical Theory and Computation* **11**, 2680 (2015).
- [50] M. Jain, J. Chelikowsky, and S. Louie, *Phys. Rev. Lett.* **107**, 216806 (2011).
- [51] M. Hybertsen and S. Louie, *Phys. Rev. B* **34**, 5390 (1986).
- [52] J. Noffsinger, E. Kioupakis, C. Van de Walle, S. Louie, and M. Cohen, *Phys. Rev. Lett.* **108**, 167402 (2012).
- [53] P. Han and G. Bester, *Phys. Rev. B* **91**, 085305 (2015).
- [54] A. Kryjevski, *Toward First-Principles Description of Carrier Relaxation in Nanoparticles in*

- Photoinduced Processes at Surfaces and in Nanomaterials, ACS Symposium Series, Vol. 1196* (2015), chap. 10, pp. 201–213.
- [55] D. T. Devreese and P. van Camp, *Electronic Structure, Dynamics, and Quantum Structural Properties of Condensed Matter* (Springer, New York, 1985).
 - [56] P. Han and G. Bester, Phys. Rev. B **85**, 235422 (2012).
 - [57] X. Gonze, P. Boulanger, and M. Cote, Annalen der Physik **523**, 168 (2011).
 - [58] A. A. Abrikosov, L. Gorkov, and I. E. Dzyaloshinski, *Methods of Quantum Field Theory in Statistical Physics* (Prentice-Hall, Englewood Cliffs, NJ, 1963).
 - [59] P. E. Blöchl, Phys. Rev. B **50**, 17953 (1994).
 - [60] G. Kresse and D. Joubert, Phys. Rev. B **59**, 1758 (1999).
 - [61] M. W. Graham, T. R. Calhoun, A. A. Green, M. C. Hersam, and G. R. Fleming, Nano Letters **12**, 813 (2012).
 - [62] C. Manzoni, A. Gambetta, E. Menna, M. Meneghetti, G. Lanzani, and G. Cerullo, Phys. Rev. Lett. **94**, 207401 (2005).
 - [63] A. Gambetta, C. Manzoni, E. Menna, M. Meneghetti, G. Cerullo, G. Lanzani, S. Tretiak, A. Piryatinski, A. Saxena, R. L. Martin, et al., Nature Physics **2**, 515 (2006).